frontiers in Oncology

MINI REVIEW
published: 18 February 2020
doi: 10.3389/fonc.2020.00161

Non-invasive Investigation of Tumor Metabolism and Acidosis by MRI-CEST Imaging

*Lorena Consolino[1,2], Annasofia Anemone[2], Martina Capozza[2], Antonella Carella[3], Pietro Irrera[4], Alessia Corrado[3], Chetan Dhakan[3,4], Martina Bracesco[2] and Dario Livio Longo[3]**

[1] Department of Nanomedicines and Theranostics, Institute for Experimental Molecular Imaging, RWTH Aachen University, Aachen, Germany, [2] Department of Molecular Biotechnology and Health Sciences, Molecular Imaging Center, University of Torino, Turin, Italy, [3] Institute of Biostructures and Bioimaging (IBB), Italian National Research Council (CNR), Turin, Italy, [4] University of Campania "Luigi Vanvitelli," Naples, Italy

Altered metabolism is considered a core hallmark of cancer. By monitoring *in vivo* metabolites changes or characterizing the tumor microenvironment, non-invasive imaging approaches play a fundamental role in elucidating several aspects of tumor biology. Within the magnetic resonance imaging (MRI) modality, the chemical exchange saturation transfer (CEST) approach has emerged as a new technique that provides high spatial resolution and sensitivity for *in vivo* imaging of tumor metabolism and acidosis. This mini-review describes CEST-based methods to non-invasively investigate tumor metabolism and important metabolites involved, such as glucose and lactate, as well as measurement of tumor acidosis. Approaches that have been exploited to assess response to anticancer therapies will also be reported for each specific technique.

Keywords: tumor metabolism, tumor acidosis, CEST-MRI, imaging, therapy, tumor pH

OPEN ACCESS

Edited by:
Alessandra Castegna, University of Bari Aldo Moro, Italy

Reviewed by:
Phillip Zhe Sun, Emory University, United States
Barbara Marengo, University of Genoa, Italy

****Correspondence:***
Dario Livio Longo
dariolivio.longo@cnr.it;
dario.longo@unito.it

Specialty section:
This article was submitted to Cancer Metabolism, a section of the journal Frontiers in Oncology

Received: *13 December 2019*
Accepted: *29 January 2020*
Published: *18 February 2020*

Citation:
Consolino L, Anemone A, Capozza M, Carella A, Irrera P, Corrado A, Dhakan C, Bracesco M and Longo DL (2020) Non-invasive Investigation of Tumor Metabolism and Acidosis by MRI-CEST Imaging. Front. Oncol. 10:161. doi: 10.3389/fonc.2020.00161

INTRODUCTION

Outgrowing tumor mass typically displays an abnormal and disorganized vascular network, with poor functional vessels and extended hypoxic region (1, 2). Hypoxia is considered one of the major driving forces of tumorigenesis through the activation of the hypoxia-inducible factor 1 (HIF-1), that directly alters the expression of genes related to cell metabolism and proliferation (3). The induced metabolic modification markedly responds to tumor requirement for survival and expansion. On one side, the upregulation of the transmembrane receptor GLUT-1 ensures increased glucose avidity as a metabolic source of proliferation (4). On the other side, the metabolic switch to the glycolytic pathway exposes tumors to the paradoxically accumulation of acidic metabolites, as lactic acid and hydrogen ions, that results to be toxic for cancer cells. Therefore, the upregulation of dedicated proton transporters allows the extrusion of acidic products on the extracellular microenvironment, guarantees the maintenance of an aberrant pH gradient and induces the adaptation and clonal expansion of the most aggressive cells able to survive in such a hostile environment (5–7).

Considering the strategic role of metabolism on tumorigenesis, several targeting therapies have been developed to interfere with tumor expansion, alone or in combination with standard therapeutic treatments (8–13). Therefore, approaches for *in vivo* assessing the response to treatments and for improving tumor diagnosis are strongly required. In the clinical setting, positron-emission tomography (PET) technique is routinely exploited for measuring glucose

uptake via 18F-fluorodeoxyglucose (FDG) injection, although radiation exposure limits repeated longitudinal studies (14–16). Furthermore, magnetic resonance imaging (MRI) offers a wide panel of approaches, by combining an optimal tissue contrast and good spatial information with acceptable sensitivity, to quantitatively interrogate several aspects of tumor microenvironment, including tumor metabolism and acidosis (17–20). One of the most promising and emerging technique for investigating tumor metabolism is the chemical exchange saturation transfer (CEST)-MRI (21, 22). CEST-MRI allows the detection of molecules endowed with mobile protons in chemical exchange with water. The application of radiofrequency (RF) pulses at specific offsets, corresponding to the absorbance peak of the mobile protons, nullifies the magnetization of the mobile protons, that become "saturated." The exchange of the saturated protons with those of water molecules results in a transfer of reduced magnetization, hence in a decrease of the water signal, generating a (negative) contrast that can be detected by MRI. Consequently, many endogenous (proteins, peptides, sugars) or exogenous molecules owing exchangeable mobile protons can be imaged by CEST-MRI (23–25).

In this mini review, we will focus on CEST-MRI as a novel tool for imaging several aspects of tumor metabolism in both preclinical and clinical settings.

IMAGING MOBILE PROTEINS (AMIDE PROTON TRANSFER: APT)

Amide proton transfer (APT) imaging is a CEST-MRI approach that can detect the amide protons of endogenous mobile proteins and peptides that resonate at 3.5 ppm (26). APT imaging has been initially exploited for studies of ischemic stroke, neurologic disorders and brain tumors (27–32). Tumors exhibit a close relationship between unregulated proliferation and concentrations of mobile proteins, that may accumulate as defective products (33). Especially in high grade malignant brain tumors, the level of peptides and mobile proteins is substantially elevated (34). In Yan et al. the APT signal was compared between normal brain tissue and tumor in rats implanted with gliosarcoma. This study demonstrated that higher APT contrast in brain tumor correlated with an increased concentration of cytosolic proteins (35). In addition, APT imaging has been used for tumor characterization and diagnosis of brain tumors in patients (36–39). Furthermore, it is possible to use this innovative technique to differentiate between malignant gliomas and malignant lymphoma (40), to discriminate solitary brain metastases from glioblastoma (41) and to predict genetic mutations in gliomas, in particular the isocitrate dehydrogenase (IDH) mutation status (42, 43). Another feature that makes APT particularly interesting is its ability to differentiate between treatment-induced effects and true tumor progression (44, 45), providing a unique and non-invasive MRI biomarker for distinguishing viable malignancy from radiation necrosis and for predicting tumor response to therapy (46). In addition to brain tumors, APT imaging has been investigated in breast and prostate cancer. As it was demonstrated in brain tumors, APT imaging is able to discriminate between prostate cancer and non-cancer tissues, reporting an increase of cell proliferation rate and cellular density in tumor regions (47). Furthermore, variations in the APT signal have been observed in breast tumors, likely reporting about therapeutic effects and transformation of breast parenchyma (48, 49). In summary, APT imaging represents a promising biomarker for monitoring tumor progression and response to treatment and can be easily implemented in existing clinical scanners, despite further work is needed to remove confounding effects (protein concentration, pH, etc.) to the observed APT contrast (50–54).

IMAGING GLUCOSE

Tumors typically display upregulated glucose uptake and glycolytic metabolism (55). In the clinical setting, PET imaging with the glucose analog FDG is considered the gold standard technique for non-invasively mapping glucose uptake and for assessing tumor response to conventional therapy (56). However, high maintenance costs and side effects related to radioactivity exposure of patients strongly limit the repeated applications of radionuclide techniques (57). Therefore, the idea of exploiting unlabeled D-glucose as an MRI contrast agent may represent a cheaper and potential alternative to FDG without involving ionizing radiations. Glucose molecules own five hydroxylic groups in fast exchange rate (500–6,000 Hz) with bulk water protons that can provide CEST contrast at 1–1.2 ppm from the water resonance (58, 59). The feasibility of imaging glucose uptake with the CEST-MRI technique was demonstrated in colorectal tumor xenograft murine models, with glucose contrast (GlucoCEST) correlated to FDG accumulation as measured by autoradiography (60). A different GlucoCEST contrast was also reported between two human breast tumor models characterized by different metabolic activity (58). In addition, the dynamic measurement of GlucoCEST contrast enhancements upon time (Dynamic Glucose Enhanced—DGE) following glucose injection showed increased penetration in brain tumors compared to the contralateral regions, demonstrating interesting application for brain tumors due to the reduced permeability of the blood brain barrier (61). One limitation of the GlucoCEST approach is the fast metabolism of native glucose that results in CEST contrast disappearance. Therefore, non-metabolizable glucose derivatives have been investigated for achieving prolonged contrast (=detectability) inside the tumor regions. Once phosphorylated by hexokinase enzymes, 2-Deoxy-D-glucose (2DG) remains entrapped in tumor cells and provides CEST contrast for long time, up to 90 min post injection (62, 63). However, the high doses required to generate enough contrast are not feasible for toxicity issues. A more promising molecule that has been intensively studied is the non-metabolizable 3-O-methyl-D-glucose (3OMG), that is considered non-toxic. Several studies tested 3OMG in different breast cancer models and showed higher uptake and CEST contrast in the more aggressive tumors, in according with the results obtained by FDG-PET (64–66). Beyond 3OMG, glucosamine (GlcN) and N-acetyl glucosamine (GlcNAc) can accumulate in tumors that

overexpress the glucose transporters GLUT1 and GLUT2. These molecules were exploited as CEST contrast agents in breast and melanoma murine cancer models with different aggressiveness showing diverse accumulation inside the tumor (67, 68). Interesting results have been also obtained with low-calorie sweeteners, like sucralose, that was shown to provide CEST contrast in glioma tumor regions, and maltitol, that showed increased enhancement in brain tumors with compromised blood brain barrier (BBB) (69, 70).

Due to the high safety profile of glucose, its first use in patients was reported as early as 2015 in a glioma patients by using a high-field (7T) scanner (71). In comparison with the conventional small molecular weight Gd-based contrast agent, different areas of contrast enhancement were detected, suggesting that D-glucose may highlight tumor regions with different perfusion or permeability properties (**Figures 1A,B**). In addition, GlucoCEST contrast time curves highlighted potentially distinct biological areas of the brain tumor 10 min after D-glucose bolus infusion (**Figures 1B,C**). Another study investigated the GlucoCEST approach in head and neck cancer patients with a 3T scanner (72). Increased GlucoCEST contrast was registered in the tumor regions compared to muscle tissue and GlucoCEST enhancements were moderately correlated with FDG-PET results, despite a spatial mismatch likely reflecting the different metabolism between FDG and glucose. To improve the sensitivity of GlucoCEST, a similar approach that exploits the chemical exchange of mobile protons based on the Spin Lock method (dubbed CESL or chemical exchange spin lock) has been proposed for detecting glucose (73, 74). First results were obtained at high fields (9.4T) with a dynamic acquisition following glucose injection in glioma patients, demonstrating the feasibility of this approach for monitoring glucose accumulation in human brain tumors. Other studies showed a different glucose uptake in tumor brain regions in comparison to normal gray matter ones at lower magnetic fields (75), thus demonstrating its translational application at clinical level (76).

Overall, these results suggest that GlucoCEST could represent a valid alternative to FDG-PET for tumor diagnosis and staging, still several limitations, including reduced detectability at low field and origin of the glucose-based contrast arising from different compartments need to be tackled in the next years (77).

IMAGING TUMOR ACIDOSIS

Intracellular Tumor pH Imaging

The amine and amide concentration-independent detection (AACID) approach is a recently developed CEST contrast mechanism that has been shown to be sensitive to intracellular pH changes (pHi). AACID CEST technique uses the ratio of the CEST effects generated by amide ($\Delta\omega = 3.50$ ppm) and amine

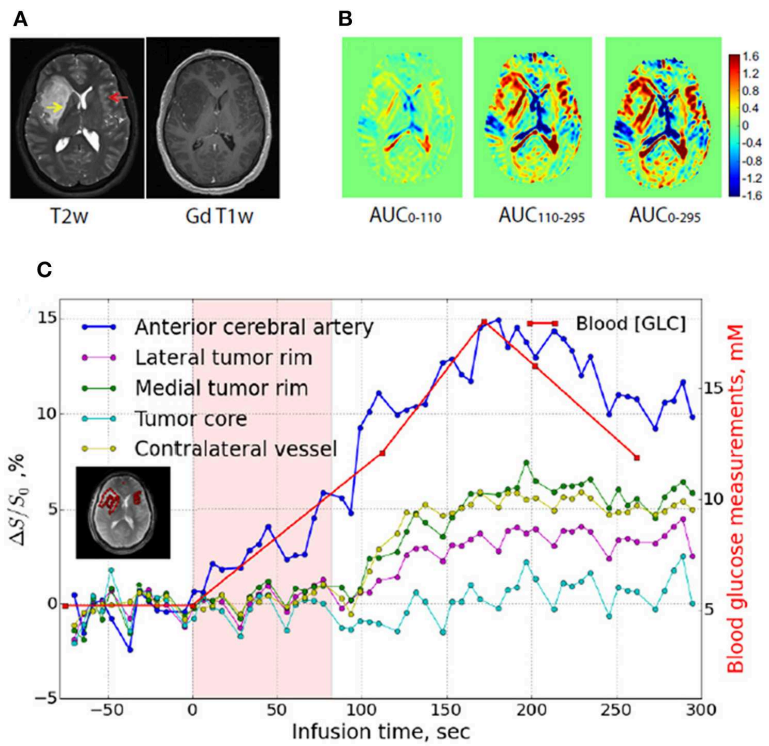

FIGURE 1 | GlucoCEST imaging in human glioma tumor. **(A)** Anatomical (T2-weighted, left) and contrast-enhanced upon Gd-injection (T1-weighted, right) MR images in a glioma patient. **(B)** GlucoCEST contrast maps calculated as Area Under the Curve (AUC) showed at several time periods (0–110 s, left panel; 110–295 s, middle panel; 0295 s, right panel) indicate progressive accumulation of glucose inside tumor. **(C)** Dynamic glucoCEST contrast time curves for several brain regions (anterior cerebral artery, tumor core, lateral tumor rim, and contralateral vessel area). These curves show that glucose accumulation in lateral and medial tumor rim starts after 100 s of infusion, whereas the enhancement in the core area does not change over time. Reproduced with permission from Xu et al. (71).

($\Delta\omega = 2.75$ ppm) protons from endogenous tissue proteins, which are predominantly from the intracellular space, for removing the concentration dependence. As a consequence, the measured CEST effect is only pH dependent, allowing to measure tumor intracellular pH (pHi) (78). McVicar et al. exploited the AACID CEST technique in a glioblastoma murine model to detect the selective acidification and decrease of pHi following the treatment with lonidamide, an anticancer drug that inhibits the monocarboxylic transporters (78). Similar results were obtained in glioblastoma murine models upon the administration of several pH-modulators such as topiramate, dichloroacetate and cariporide (79–82).

Another non-invasive pH-weighted imaging technique is the amine CEST approach, in which the amine protons (resonating at 3 ppm) of glutamine or glutamate molecules provide a pH-dependent (but not concentration independent) CEST contrast for mapping acidic tumor regions. Harris et al. applied this approach in both glioma murine models and in glioblastoma patients to detect acidic tumors and response to bevacizumab treatment (83, 84). Although the high translational potential of these endogenous approaches, concerns related to their capability to distinguish between intra- and extracellular pH contribution are still under consideration. In addition, variation of amide protons concentrations might be responsible of confounding effects resulting in less reliable pH estimations.

A recent approach to uncouple the contribution of concentration and exchange rate to the measured CEST contrast is that based on the omega-plot technique, initially developed to assess chemical exchange rates in paramagnetic contrast agents (85). Such approach has been improved and exploited for diamagnetic molecules *in vitro* (simulating complex endogenous systems) by simultaneous determination of labile proton ratio and exchange rate (that is dependent on pH) (86, 87). Although not yet demonstrated, the omega plot approach may provide useful information for intracellular pH, but further technical advancements are needed to translate it *in vivo*.

Extracellular Tumor pH Imaging

To overcome the limitations of endogenous CEST-MRI techniques, exogenous molecules have been exploited as extracellular tumor pH reporters for CEST-MRI applications. In the last decade, great expectations surrounded the class of the X-ray FDA-approved iodinated contrast media, considering their high safety profile and translational potential (88). Due to their hydrophilic chemical structure, iodinated agents remain confined outside the cells and can be visualized as perfusion agents in tumor by CEST-MRI (89, 90). Their first application as pH CEST-MRI agents involved the use of iopamidol (Isovue®, Bracco Diagnostic), possessing two amide proton pools that can be saturated at 4.2 and 5.5 ppm (91, 92). The set-up of a ratiometric procedure allows to accurately measure extracellular tissue pH (pHe) in the pH range of 5.5–7.9, independently of the contrast agent concentration, with an accuracy of 0.1 units at several magnetic fields (93–95). CEST-MRI tumor pH imaging was combined to FDG-PET to elucidate the deregulation of tumor metabolism in a breast cancer model (96). This work evidenced that tumor regions with more acidic pHe show increased FDG uptake and demonstrated *in vivo*, for the first time, the relationship between tumor acidosis and high glycolytic rate. In addition, it provided evidence of the feasibility of measuring tumor pH heterogeneity at the clinical field of 3T (**Figures 2A,B**). The combination of CEST pH-imaging and FDG-PET was then exploited for predicting the early therapeutic efficacy of metformin in a preclinical model of pancreatic cancer (98). In addition, the possibility to measure tumor pHe opened new routes for monitoring the effect of novel anticancer treatments that can reverse the glycolytic tumor phenotype (97). Anemone et al. showed that this approach can monitor early pH changes in a breast murine cancer model upon the treatment with dichloroacetate, a small compound targeting mitochondria, and that can be exploited to detect the onset of the resistance, hence providing useful insights about the therapeutic efficacy (**Figures 2C,D**).

Another iodinated agent used for pH mapping is iopromide (Ultravist®, Bayer Healthcare), that has two amide pools resonating at 4.6 and 5.6 ppm that can be exploited to measure tumor pH within the 6.5–7.2 range (99). CEST-MRI with iopromide revealed that breast cancer models with different histopathological features show significant differences in pHe values and that tumor acidosis is associated with metabolic biomarkers in B-lymphoma xenografts (100, 101). In addition, a comparative study between iopromide and iopamidol showed that although these agents measured similar pH values *in vivo*, iopamidol reveals more accurate pH measurement (102).

One of the main advantages of this class of agents relies in their very high safety profile for administration in patients. Consequently, CEST-MRI pH imaging with iopamidol was initially translated for measuring kidney and bladder pH in healthy volunteers (103–105). Later on, the capability to provide accurate tumor pH maps was demonstrated with iopamidol in both breast and ovarian cancer patients showing acidic tumor pH values (106). These preliminary results pointed out that efficient translation still requires optimization of several aspects, including acquisition protocol and data analysis to further evaluate the diagnostic and therapeutic utility of tumor pH mapping in the clinical setting. To this purpose, different studies aimed to optimize RF irradiation, reduce respiration artifacts and enlarge the body coverage acquisition have been performed (107–109). In addition, new ratiometric approaches have been formulated to extend the use of iodinated agents even with a single resonating protons for pH measurements (110, 111). Promising results have been obtained with iobitridol (Xenetix®, Guerbet), showing accurate pH measurement in murine tumors once irradiated with different power levels (112).

PARACEST pH-responsive agents are characterized by a large chemical shift of the mobile protons from the water peak that should improve their detectability in comparison to DIACEST molecules, as iodinated agents or glucose (23, 113). The Yb-HPDO3A contrast agent has been exploited for measuring tumor pHe in both melanoma and in glioma murine models (114, 115). Interestingly, in the melanoma model changes in tumor pHe were observed and correlated with the tumor progression stage. Similar approaches based on other PARACEST agents allowed to measure tumor pHe in rat brain tumor models,

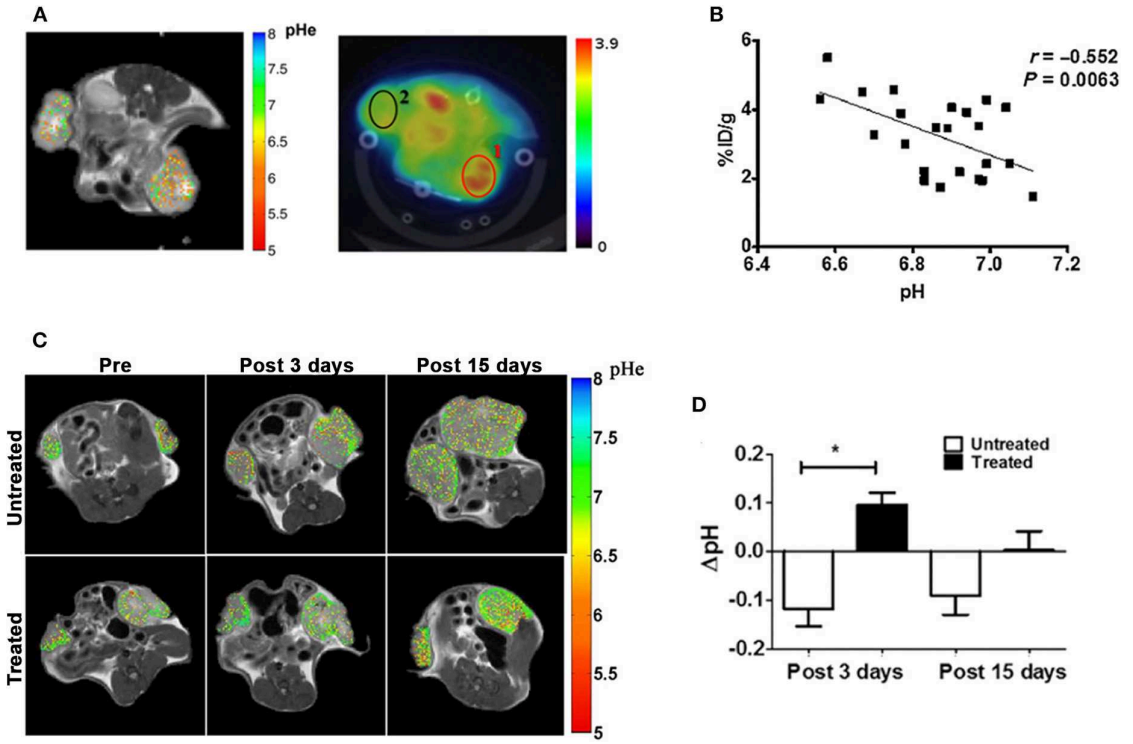

FIGURE 2 | MRI-CEST tumor pH imaging upon iopamidol injection in murine tumors. **(A)** CEST-MRI pHe maps of a breast cancer tumor overlaid on anatomical MRI image upon iopamidol injection (left) and FDG-PET image overlaid on CT image (middle) upon FDG injection in the same mouse. The tumor on the right side shows lower pHe values in the MRI-CEST pHe map corresponding to higher FDG uptake in the PET image. **(B)** Correlation plot between FDG-PET uptake and tumor pHe values shows a significant inverse correlation between FDG uptake (% ID/g) and tumor pH values. Reproduced with permission from Longo et al. (96). **(C)** Representative CEST-MRI tumor pHe maps overimposed on anatomical reference images before, 3 and 15 days after treatment with dichloroacetate for treated and untreated mice. Images show increased number of less acidic pixel in treated tumors upon dichloracetate therapy in comparison to control mates. **(D)** Bar graphs show a significant reduction in tumor acidosis after 3 days of treatment in treated tumors compared to untreated mates, whereas a restoration of tumor acidosis, likely reflecting the onset of tumor resistance is reported after 15 days of treatment (*$P < 0.05$, Student's t test). Reproduced with permission from Anemone et al. (97).

although direct injection of the contrast agent in the tumor and renal ligation were needed to maintain high concentrations of the agent for measuring pH (116–118). Currently, the high saturation power needed to generate enough CEST contrast limits a wider applicability of these pH responsive PARACEST agents, however molecules with optimal exchange rates have been recently proposed (119).

IMAGING LACTATE

The preferential ATP production via glycolysis of glucose to lactate leads to high lactate levels that some cancer cells can even exploit as a metabolic fuel (120–122). Conventionally, lactate can be observed and quantified by Magnetic Resonance Spectroscopy (MRS) or by the recently developed hyperpolarization technique (123–129). However, these methods are limited by low spatial resolution and long acquisition times. The chemical shift of the hydroxylic proton of the lactate is very close to the water signal and renders quite difficult to directly detect lactate *in vivo* by CEST imaging. However, correlation of the signal arising from lactate between CEST and MR spectroscopy has been performed in a lymphoma murine tumor upon lactate infusion (130) or in a mitochondrial disease model (131). Other approaches exploited lactate-responsive PARACEST contrast agents for taking advantage of the larger chemical shift difference of these molecules and the CEST contrast dependence with lactate concentration (132, 133). Zhang et al. (134) demonstrated the feasibility of this approach by measuring lactate excreted from lung cancer cells in tissue culture.

CONCLUSION AND FUTURE PERSPECTIVES

In summary, CEST-MRI imaging is a fast-expanding field with enormous potential to assess several aspects of tumor metabolism. Moreover, since tumor acidosis is a general feature in all tumors, imaging tumor pH might become a powerful and wide tool for oncological imaging at both preclinical and clinical level. First studies in patients demonstrated the feasibility of these novel imaging approaches for imaging human tumors. Further improvements in fast acquisition sequences, post-processing and standardization set-up are mandatory for the widespread use of CEST-MRI in the clinical settings. Despite the fundamental insights that imaging tumor acidosis with iopamidol can provide,

additional studies are needed to validate it in comparison to established clinical approaches and to demonstrate that it can be exploited for monitoring treatment response to (novel) anticancer therapies.

AUTHOR CONTRIBUTIONS

DL and LC conceived, structured, and edited the mini review article. DL, LC, AA, MC, ACa, PI, CD, ACo, and MB each wrote individual sections of the mini review article and critically revised it for intellectual content. All authors provided final approval of the version of the article submitted for publication.

FUNDING

We gratefully acknowledge the support of the Associazione Italiana Ricerca Cancro (AIRC MFAG #20153 to DL) and Compagnia San Paolo project (Regione Piemonte, grant #CSTO165925) and from the European Union's Horizon 2020 research and innovation programme (Grant Agreement No. 667510) funding. LC was supported by the AIRC fellowship for abroad Monica Broggi. The Italian Ministry for Education and Research (MIUR) is gratefully acknowledged for yearly FOE funding to the Euro-BioImaging Multi-Modal Molecular Imaging Italian Node (MMMI).

REFERENCES

1. Balkwill FR, Capasso M, Hagemann T. The tumor microenvironment at a glance. *J Cell Sci.* (2012) 125(Pt 23):5591–6. doi: 10.1242/jcs.116392
2. Carmeliet P, Jain RK. Angiogenesis in cancer and other diseases. *Nature.* (2000) 407:249–57. doi: 10.1038/35025220
3. Vaupel P. Metabolic microenvironment of tumor cells: a key factor in malignant progression. *Exp Oncol.* (2010) 32:125–7.
4. Gatenby RA, Gillies RJ. Why do cancers have high aerobic glycolysis? *Nat Rev Cancer.* (2004) 4:891–9. doi: 10.1038/nrc1478
5. Corbet C, Feron O. Tumour acidosis: from the passenger to the driver's seat. *Nat Rev Cancer.* (2017) 17:577–93. doi: 10.1038/nrc.2017.77
6. Damaghi M, Wojtkowiak JW, Gillies RJ. pH sensing and regulation in cancer. *Front Physiol.* (2013) 4:370. doi: 10.3389/fphys.2013.00370
7. Estrella V, Chen T, Lloyd M, Wojtkowiak J, Cornnell HH, Ibrahim-Hashim A, et al. Acidity generated by the tumor microenvironment drives local invasion. *Cancer Res.* (2013) 73:1524–35. doi: 10.1158/0008-5472.CAN-12-2796
8. Ganapathy-Kanniappan S, Geschwind JF. Tumor glycolysis as a target for cancer therapy: progress and prospects. *Mol Cancer.* (2013) 12:152. doi: 10.1186/1476-4598-12-152
9. Neri D, Supuran CT. Interfering with pH regulation in tumours as a therapeutic strategy. *Nat Rev Drug Discov.* (2011) 10:767–77. doi: 10.1038/nrd3554
10. Pillai SR, Damaghi M, Marunaka Y, Spugnini EP, Fais S, Gillies RJ. Causes, consequences, and therapy of tumors acidosis. *Cancer Metastasis Rev.* (2019) 38:205–22. doi: 10.1007/s10555-019-09792-7
11. Kolosenko I, Avnet S, Baldini N, Viklund J, De Milito A. Therapeutic implications of tumor interstitial acidification. *Semin Cancer Biol.* (2017) 43:119–33. doi: 10.1016/j.semcancer.2017.01.008
12. Harguindey S, Arranz JL, Wahl ML, Orive G, Reshkin SJ. Proton transport inhibitors as potentially selective anticancer drugs. *Anticancer Res.* (2009) 29:2127–36.
13. De Milito A, Fais S. Tumor acidity, chemoresistance and proton pump inhibitors. *Future Oncol.* (2005) 1:779–86. doi: 10.2217/14796694.1.6.779
14. Zhu A, Lee D, Shim H. Metabolic positron emission tomography imaging in cancer detection and therapy response. *Semin Oncol.* (2011) 38:55–69. doi: 10.1053/j.seminoncol.2010.11.012
15. Pantel AR, Ackerman D, Lee SC, Mankoff DA, Gade TP. Imaging cancer metabolism: underlying biology and emerging strategies. *J Nucl Med.* (2018) 59:1340–9. doi: 10.2967/jnumed.117.199869
16. Apostolova I, Wedel F, Brenner W. Imaging of tumor metabolism using positron emission tomography (PET). *Recent Results Cancer Res.* (2016) 207:177–205. doi: 10.1007/978-3-319-42118-6_8
17. Anemone A, Consolino L, Arena F, Capozza M, Longo DL. Imaging tumor acidosis: a survey of the available techniques for mapping *in vivo* tumor pH. *Cancer Metastasis Rev.* (2019) 38:25–49. doi: 10.1007/s10555-019-09782-9
18. Li Y, Park I, Nelson SJ. Imaging tumor metabolism using *in vivo* magnetic resonance spectroscopy. *Cancer J.* (2015) 21:123–8. doi: 10.1097/PPO.0000000000000097
19. Matsuo M, Matsumoto S, Mitchell JB, Krishna MC, Camphausen K. Magnetic resonance imaging of the tumor microenvironment in radiotherapy: perfusion, hypoxia, and metabolism. *Semin Radiat Oncol.* (2014) 24:210–7. doi: 10.1016/j.semradonc.2014.02.002
20. Ramamonjisoa N, Ackerstaff E. Characterization of the tumor microenvironment and tumor-stroma interaction by non-invasive preclinical imaging. *Front Oncol.* (2017) 7:3. doi: 10.3389/fonc.2017.00003
21. van Zijl PC, Yadav NN. Chemical exchange saturation transfer (CEST): what is in a name and what isn't? *Magn Reson Med.* (2011) 65:927–48. doi: 10.1002/mrm.22761
22. Wu B, Warnock G, Zaiss M, Lin C, Chen M, Zhou Z, et al. An overview of CEST MRI for non-MR physicists. *EJNMMI Phys.* (2016) 3:19. doi: 10.1186/s40658-016-0155-2
23. Vinogradov E, Sherry AD, Lenkinski RE. CEST: from basic principles to applications, challenges and opportunities. *J Magn Reson.* (2013) 229:155–72. doi: 10.1016/j.jmr.2012.11.024
24. Liu G, Song X, Chan KW, McMahon MT. Nuts and bolts of chemical exchange saturation transfer MRI. *NMR Biomed.* (2013) 26:810–28. doi: 10.1002/nbm.2899
25. Longo DL, Di Gregorio E, Abategiovanni R, Ceccon A, Assfalg M, Molinari H, et al. Chemical exchange saturation transfer (CEST): an efficient tool for detecting molecular information on proteins' behaviour. *Analyst.* (2014) 139:2687–90. doi: 10.1039/C4AN00346B
26. Zhou J, Payen JF, Wilson DA, Traystman RJ, van Zijl PC. Using the amide proton signals of intracellular proteins and peptides to detect pH effects in MRI. *Nat Med.* (2003) 9:1085–90. doi: 10.1038/nm907
27. Zhou J. Amide proton transfer imaging of the human brain. *Methods Mol Biol.* (2011) 711:227–37. doi: 10.1007/978-1-61737-992-5_10
28. Yu L, Chen Y, Chen M, Luo X, Jiang S, Zhang Y, et al. Amide proton transfer MRI signal as a surrogate biomarker of ischemic stroke recovery in patients with supportive treatment. *Front Neurol.* (2019) 10:104. doi: 10.3389/fneur.2019.00104
29. Holmes HE, Colgan N, Ismail O, Ma D, Powell NM, O'Callaghan JM, et al. Imaging the accumulation and suppression of tau pathology using multiparametric MRI. *Neurobiol Aging.* (2016) 39:184–94. doi: 10.1016/j.neurobiolaging.2015.12.001
30. Wells JA, O'Callaghan JM, Holmes HE, Powell NM, Johnson RA, Siow B, et al. *In vivo* imaging of tau pathology using multi-parametric quantitative MRI. *Neuroimage.* (2015) 111:369–78. doi: 10.1016/j.neuroimage.2015.02.023
31. Zhou J, Lal B, Wilson DA, Laterra J, van Zijl PC. Amide proton transfer (APT) contrast for imaging of brain tumors. *Magn Reson Med.* (2003) 50:1120–6. doi: 10.1002/mrm.10651
32. Sun PZ, Zhou J, Sun W, Huang J, van Zijl PC. Detection of the ischemic penumbra using pH-weighted MRI. *J Cereb Blood Flow Metab.* (2007) 27:1129–36. doi: 10.1038/sj.jcbfm.9600424
33. Salhotra A, Lal B, Laterra J, Sun PZ, van Zijl PC, Zhou J. Amide proton transfer imaging of 9L gliosarcoma and human glioblastoma xenografts. *NMR Biomed.* (2008) 21:489–97. doi: 10.1002/nbm.1216
34. Hobbs SK, Shi G, Homer R, Harsh G, Atlas SW, Bednarski MD. Magnetic resonance image-guided proteomics of human glioblastoma multiforme. *J Magn Reson Imaging.* (2003) 18:530–6. doi: 10.1002/jmri.10395

35. Yan K, Fu Z, Yang C, Zhang K, Jiang S, Lee DH, et al. Assessing amide proton transfer (APT) MRI contrast origins in 9 L gliosarcoma in the rat brain using proteomic analysis. *Mol Imaging Biol.* (2015) 17:479–87. doi: 10.1007/s11307-015-0828-6
36. Togao O, Yoshiura T, Keupp J, Hiwatashi A, Yamashita K, Kikuchi K, et al. Amide proton transfer imaging of adult diffuse gliomas: correlation with histopathological grades. *Neuro Oncol.* (2014) 16:441–8. doi: 10.1093/neuonc/not158
37. Jones CK, Schlosser MJ, van Zijl PC, Pomper MG, Golay X, Zhou J. Amide proton transfer imaging of human brain tumors at 3T. *Magn Reson Med.* (2006) 56:585–92. doi: 10.1002/mrm.20989
38. Choi YS, Ahn SS, Lee SK, Chang JH, Kang SG, Kim SH, et al. Amide proton transfer imaging to discriminate between low- and high-grade gliomas: added value to apparent diffusion coefficient and relative cerebral blood volume. *Eur Radiol.* (2017) 27:3181–9. doi: 10.1007/s00330-017-4732-0
39. Sakata A, Fushimi Y, Okada T, Arakawa Y, Kunieda T, Minamiguchi S, et al. Diagnostic performance between contrast enhancement, proton MR spectroscopy, and amide proton transfer imaging in patients with brain tumors. *J Magn Reson Imaging.* (2017) 46:732–9. doi: 10.1002/jmri.25597
40. Jiang S, Yu H, Wang X, Lu S, Li Y, Feng L, et al. Molecular MRI differentiation between primary central nervous system lymphomas and high-grade gliomas using endogenous protein-based amide proton transfer MR imaging at 3 Tesla. *Eur Radiol.* (2016) 26:64–71. doi: 10.1007/s00330-015-3805-1
41. Yu H, Lou H, Zou T, Wang X, Jiang S, Huang Z, et al. Applying protein-based amide proton transfer MR imaging to distinguish solitary brain metastases from glioblastoma. *Eur Radiol.* (2017) 27:4516–24. doi: 10.1007/s00330-017-4867-z
42. Jiang S, Zou T, Eberhart CG, Villalobos MAV, Heo HY, Zhang Y, et al. Predicting IDH mutation status in grade II gliomas using amide proton transfer-weighted (APTw) MRI. *Magn Reson Med.* (2017) 78:1100–9. doi: 10.1002/mrm.26820
43. Paech D, Windschuh J, Oberhollenzer J, Dreher C, Sahm F, Meissner JE, et al. Assessing the predictability of IDH mutation and MGMT methylation status in glioma patients using relaxation-compensated multipool CEST MRI at 7.0 T. *Neuro Oncol.* (2018) 20:1661–71. doi: 10.1093/neuonc/noy073
44. Ma B, Blakeley JO, Hong X, Zhang H, Jiang S, Blair L, et al. Applying amide proton transfer-weighted MRI to distinguish pseudoprogression from true progression in malignant gliomas. *J Magn Reson Imaging.* (2016) 44:456–62. doi: 10.1002/jmri.25159
45. Jiang S, Eberhart CG, Lim M, Heo HY, Zhang Y, Blair L, et al. Identifying recurrent malignant glioma after treatment using amide proton transfer-weighted MR imaging: a validation study with image-guided stereotactic biopsy. *Clin Cancer Res.* (2019) 25:552–61. doi: 10.1158/1078-0432.CCR-18-1233
46. Zhou J, Tryggestad E, Wen Z, Lal B, Zhou T, Grossman R, et al. Differentiation between glioma and radiation necrosis using molecular magnetic resonance imaging of endogenous proteins and peptides. *Nat Med.* (2011) 17:130–4. doi: 10.1038/nm.2268
47. Jia G, Abaza R, Williams JD, Zynger DL, Zhou J, Shah ZK, et al. Amide proton transfer MR imaging of prostate cancer: a preliminary study. *J Magn Reson Imaging.* (2011) 33:647–54. doi: 10.1002/jmri.22480
48. Krikken E, Khlebnikov V, Zaiss M, Jibodh RA, van Diest PJ, Luijten PR, et al. Amide chemical exchange saturation transfer at 7 T: a possible biomarker for detecting early response to neoadjuvant chemotherapy in breast cancer patients. *Breast Cancer Res.* (2018) 20:51. doi: 10.1186/s13058-018-0982-2
49. Dula AN, Arlinghaus LR, Dortch RD, Dewey BE, Whisenant JG, Ayers GD, et al. Amide proton transfer imaging of the breast at 3 T: establishing reproducibility and possible feasibility assessing chemotherapy response. *Magn Reson Med.* (2013) 70:216–24. doi: 10.1002/mrm.24450
50. Zaiss M, Windschuh J, Paech D, Meissner JE, Burth S, Schmitt B, et al. Relaxation-compensated CEST-MRI of the human brain at 7T: Unbiased insight into NOE and amide signal changes in human glioblastoma. *Neuroimage.* (2015) 112:180–8. doi: 10.1016/j.neuroimage.2015.02.040
51. Windschuh J, Zaiss M, Meissner JE, Paech D, Radbruch A, Ladd ME, et al. Correction of B1-inhomogeneities for relaxation-compensated CEST imaging at 7 T. *NMR Biomed.* (2015) 28:529–37. doi: 10.1002/nbm.3283
52. Zaiss M, Xu J, Goerke S, Khan IS, Singer RJ, Gore JC, et al. Inverse Z-spectrum analysis for spillover-, MT-, and T1 -corrected steady-state pulsed CEST-MRI–application to pH-weighted MRI of acute stroke. *NMR Biomed.* (2014) 27:240–52. doi: 10.1002/nbm.3054
53. Yuwen Zhou I, Wang E, Cheung JS, Lu D, Ji Y, Zhang X, et al. Direct saturation-corrected chemical exchange saturation transfer MRI of glioma: simplified decoupling of amide proton transfer and nuclear overhauser effect contrasts. *Magn Reson Med.* (2017) 78:2307–14. doi: 10.1002/mrm.26959
54. Wu Y, Chen Y, Zhao Y, Yang S, Zhao J, Zhou J, et al. Direct radiofrequency saturation corrected amide proton transfer tumor MRI at 3T. *Magn Reson Med.* (2019) 81:2710–9. doi: 10.1002/mrm.27562
55. Goldenberg JM, Pagel MD. Assessments of tumor metabolism with CEST MRI. *NMR Biomed.* (2019) 32:e3943. doi: 10.1002/nbm.3943
56. Gambhir SS. Molecular imaging of cancer with positron emission tomography. *Nat Rev Cancer.* (2002) 2:683–93. doi: 10.1038/nrc882
57. Gambhir SS, Czernin J, Schwimmer J, Silverman DH, Coleman RE, Phelps ME. A tabulated summary of the FDG PET literature. *J Nucl Med.* (2001) 42(5 Suppl):1S—93S.
58. Chan KW, McMahon MT, Kato Y, Liu G, Bulte JW, Bhujwalla ZM, et al. Natural D-glucose as a biodegradable MRI contrast agent for detecting cancer. *Magn Reson Med.* (2012) 68:1764–73. doi: 10.1002/mrm.24520
59. Zaiss M, Anemone A, Goerke S, Longo DL, Herz K, Pohmann R, et al. Quantification of hydroxyl exchange of D-Glucose at physiological conditions for optimization of glucoCEST MRI at 3, 7 and 9.4 Tesla. *NMR Biomed.* (2019) 32:e4113. doi: 10.1002/nbm.4113
60. Walker-Samuel S, Ramasawmy R, Torrealdea F, Rega M, Rajkumar V, Johnson SP, et al. *In vivo* imaging of glucose uptake and metabolism in tumors. *Nat Med.* (2013) 19:1067–72. doi: 10.1038/nm.3252
61. Xu X, Chan KW, Knutsson L, Artemov D, Xu J, Liu G, et al. Dynamic glucose enhanced (DGE) MRI for combined imaging of blood-brain barrier break down and increased blood volume in brain cancer. *Magn Reson Med.* (2015) 74:1556–63. doi: 10.1002/mrm.25995
62. Nasrallah FA, Pages G, Kuchel PW, Golay X, Chuang KH. Imaging brain deoxyglucose uptake and metabolism by glucoCEST MRI. *J Cereb Blood Flow Metab.* (2013) 33:1270–8. doi: 10.1038/jcbfm.2013.79
63. Rivlin M, Horev J, Tsarfaty I, Navon G. Molecular imaging of tumors and metastases using chemical exchange saturation transfer (CEST) MRI. *Sci Rep.* (2013) 3:3045. doi: 10.1038/srep03045
64. Rivlin M, Tsarfaty I, Navon G. Functional molecular imaging of tumors by chemical exchange saturation transfer MRI of 3-O-Methyl-D-glucose. *Magn Reson Med.* (2014) 72:1375–80. doi: 10.1002/mrm.25467
65. Rivlin M, Navon G. 3-O-Methyl-D-glucose mutarotation and proton exchange rates assessed by (13)C, (1)H NMR and by chemical exchange saturation transfer and spin lock measurements. *J Biomol NMR.* (2018) 72:93–103. doi: 10.1007/s10858-018-0209-y
66. Rivlin M, Navon G. CEST MRI of 3-O-methyl-D-glucose on different breast cancer models. *Magn Reson Med.* (2018) 79:1061–9. doi: 10.1002/mrm.26752
67. Rivlin M, Navon G. Glucosamine and N-acetyl glucosamine as new CEST MRI agents for molecular imaging of tumors. *Sci Rep.* (2016) 6:32648. doi: 10.1038/srep32648
68. Longo DL, Moustaghfir FZ, Zerbo A, Consolino L, Anemone A, Bracesco M, et al. EXCI-CEST: Exploiting pharmaceutical excipients as MRI-CEST contrast agents for tumor imaging. *Int J Pharm.* (2017) 525:275–81. doi: 10.1016/j.ijpharm.2017.04.040
69. Bagga P, Haris M, D'Aquilla K, Wilson NE, Marincola FM, Schnall MD, et al. Non-caloric sweetener provides magnetic resonance imaging contrast for cancer detection. *J Transl Med.* (2017) 15:119. doi: 10.1186/s12967-017-1221-9
70. Bagga P, Wilson N, Rich L, Marincola FM, Schnall MD, Hariharan H, et al. Sugar alcohol provides imaging contrast in cancer detection. *Sci Rep.* (2019) 9:11092. doi: 10.1038/s41598-019-47275-5
71. Xu X, Yadav NN, Knutsson L, Hua J, Kalyani R, Hall E, et al. Dynamic glucose-enhanced (DGE) MRI: translation to human scanning and first results in glioma patients. *Tomography.* (2015) 1:105–14. doi: 10.18383/j.tom.2015.00175
72. Wang J, Weygand J, Hwang KP, Mohamed AS, Ding Y, Fuller CD, et al. Magnetic resonance imaging of glucose uptake and metabolism in patients with head and neck cancer. *Sci Rep.* (2016) 6:30618. doi: 10.1038/srep30618
73. Schuenke P, Koehler C, Korzowski A, Windschuh J, Bachert P, Ladd ME, et al. Adiabatically prepared spin-lock approach for T1rho-based dynamic glucose

enhanced MRI at ultrahigh fields. *Magn Reson Med.* (2017) 78:215–25. doi: 10.1002/mrm.26370
74. Schuenke P, Paech D, Koehler C, Windschuh J, Bachert P, Ladd ME, et al. Fast and quantitative T1rho-weighted dynamic glucose enhanced MRI. *Sci Rep.* (2017) 7:42093. doi: 10.1038/srep42093
75. Paech D, Schuenke P, Koehler C, Windschuh J, Mundiyanapurath S, Bickelhaupt S, et al. T1rho-weighted dynamic glucose-enhanced MR imaging in the human brain. *Radiology.* (2017) 285:914–22. doi: 10.1148/radiol.2017162351
76. Herz K, Lindig T, Deshmane A, Schittenhelm J, Skardelly M, Bender B, et al. T1rho-based dynamic glucose-enhanced (DGErho) MRI at 3 T: method development and early clinical experience in the human brain. *Magn Reson Med.* (2019) 82:1832–47. doi: 10.1002/mrm.27857
77. Kim M, Torrealdea F, Adeleke S, Rega M, Evans V, Beeston T, et al. Challenges in glucoCEST MR body imaging at 3 Tesla. *Quant Imag Med Surg.* (2019) 9:1628–40. doi: 10.21037/qims.2019.10.05
78. McVicar N, Li AX, Meakin SO, Bartha R. Imaging chemical exchange saturation transfer (CEST) effects following tumor-selective acidification using lonidamine. *NMR Biomed.* (2015) 28:566–75. doi: 10.1002/nbm.3287
79. Marathe K, McVicar N, Li A, Bellyou M, Meakin S, Bartha R. Topiramate induces acute intracellular acidification in glioblastoma. *J Neurooncol.* (2016) 130:465–72. doi: 10.1007/s11060-016-2258-y
80. Albatany M, Li A, Meakin S, Bartha R. Dichloroacetate induced intracellular acidification in glioblastoma: *in vivo* detection using AACID-CEST MRI at 9.4 Tesla. *J Neurooncol.* (2018) 136:255–62. doi: 10.1007/s11060-017-2664-9
81. Albatany M, Li A, Meakin S, Bartha R. *In vivo* detection of acute intracellular acidification in glioblastoma multiforme following a single dose of cariporide. *Int J Clin Oncol.* (2018) 23:812–9. doi: 10.1007/s10147-018-1289-0
82. Albatany M, Ostapchenko VG, Meakin S, Bartha R. Brain tumor acidification using drugs simultaneously targeting multiple pH regulatory mechanisms. *J Neurooncol.* (2019) 144:453–62. doi: 10.1007/s11060-019-03251-7
83. Harris RJ, Cloughesy TF, Liau LM, Prins RM, Antonios JP, Li D, et al. pH-weighted molecular imaging of gliomas using amine chemical exchange saturation transfer MRI. *Neuro Oncol.* (2015) 17:1514–24. doi: 10.1093/neuonc/nov106
84. Yao J, Tan CHP, Schlossman J, Chakhoyan A, Raymond C, Pope WB, et al. pH-weighted amine chemical exchange saturation transfer echoplanar imaging (CEST-EPI) as a potential early biomarker for bevacizumab failure in recurrent glioblastoma. *J Neurooncol.* (2019) 142:587–95. doi: 10.1007/s11060-019-03132-z
85. Dixon WT, Ren J, Lubag AJ, Ratnakar J, Vinogradov E, Hancu I, et al. A concentration-independent method to measure exchange rates in PARACEST agents. *Magn Reson Med.* (2010) 63:625–32. doi: 10.1002/mrm.22242
86. Wu R, Xiao G, Zhou IY, Ran C, Sun PZ. Quantitative chemical exchange saturation transfer (qCEST) MRI - omega plot analysis of RF-spillover-corrected inverse CEST ratio asymmetry for simultaneous determination of labile proton ratio and exchange rate. *NMR Biomed.* (2015) 28:376–83. doi: 10.1002/nbm.3257
87. Sun PZ, Wang Y, Dai Z, Xiao G, Wu R. Quantitative chemical exchange saturation transfer (qCEST) MRI–RF spillover effect-corrected omega plot for simultaneous determination of labile proton fraction ratio and exchange rate. *Contrast Media Mol Imaging.* (2014) 9:268–75. doi: 10.1002/cmmi.1569
88. Longo D, Aime S. Iodinated contrast media as pH-Responsive CEST agents. In: McMahon MT, Gilad AA, Bulte JBM, Van Zijl PCM, editors. *Chemical Exchange Saturation Transfer Imaging*. Singapore: Pan Stanford Publishing (2017). p. 447–66. doi: 10.1201/9781315364421-20
89. Longo DL, Michelotti F, Consolino L, Bardini P, Digilio G, Xiao G, et al. *In vitro* and *in vivo* assessment of nonionic iodinated radiographic molecules as chemical exchange saturation transfer magnetic resonance imaging tumor perfusion agents. *Invest Radiol.* (2016) 51:155–62. doi: 10.1097/RLI.0000000000000217
90. Anemone A, Consolino L, Longo DL. MRI-CEST assessment of tumour perfusion using X-ray iodinated agents: comparison with a conventional Gd-based agent. *Eur Radiol.* (2017) 27:2170–9. doi: 10.1007/s00330-016-4552-7
91. Longo DL, Dastru W, Digilio G, Keupp J, Langereis S, Lanzardo S, et al. Iopamidol as a responsive MRI-chemical exchange saturation transfer contrast agent for pH mapping of kidneys: *in vivo* studies in mice at 7 T. *Magn Reson Med.* (2011) 65:202–11. doi: 10.1002/mrm.22608
92. Aime S, Calabi L, Biondi L, De Miranda M, Ghelli S, Paleari L, et al. Iopamidol: exploring the potential use of a well-established x-ray contrast agent for MRI. *Magn Reson Med.* (2005) 53:830–4. doi: 10.1002/mrm.20441
93. Longo DL, Busato A, Lanzardo S, Antico F, Aime S. Imaging the pH evolution of an acute kidney injury model by means of iopamidol, a MRI-CEST pH-responsive contrast agent. *Magn Reson Med.* (2013) 70:859–64. doi: 10.1002/mrm.24513
94. Longo DL, Cutrin JC, Michelotti F, Irrera P, Aime S. Noninvasive evaluation of renal pH homeostasis after ischemia reperfusion injury by CEST-MRI. *NMR Biomed.* (2017) 30:e3720. doi: 10.1002/nbm.3720
95. Wu Y, Zhou IY, Igarashi T, Longo DL, Aime S, Sun PZ. A generalized ratiometric chemical exchange saturation transfer (CEST) MRI approach for mapping renal pH using iopamidol. *Magn Reson Med.* (2018) 79:1553–8. doi: 10.1002/mrm.26817
96. Longo DL, Bartoli A, Consolino L, Bardini P, Arena F, Schwaiger M, et al. *In vivo* imaging of tumor metabolism and acidosis by combining PET and MRI-CEST pH imaging. *Cancer Res.* (2016) 76:6463–70. doi: 10.1158/0008-5472.CAN-16-0825
97. Anemone A, Consolino L, Conti L, Reineri F, Cavallo F, Aime S, et al. *In vivo* evaluation of tumour acidosis for assessing the early metabolic response and onset of resistance to dichloroacetate by using magnetic resonance pH imaging. *Int J Oncol.* (2017) 51:498–506. doi: 10.3892/ijo.2017.4029
98. Goldenberg JM, Cardenas-Rodriguez J, Pagel MD. Preliminary results that assess metformin treatment in a preclinical model of pancreatic cancer using simultaneous [(18)F]FDG PET and acidoCEST MRI. *Mol Imaging Biol.* (2018) 20:575–83. doi: 10.1007/s11307-018-1164-4
99. Chen LQ, Howison CM, Jeffery JJ, Robey IF, Kuo PH, Pagel MD. Evaluations of extracellular pH within *in vivo* tumors using acidoCEST MRI. *Magn Reson Med.* (2014) 72:1408–17. doi: 10.1002/mrm.25053
100. Chen LQ, Randtke EA, Jones KM, Moon BF, Howison CM, Pagel MD. Evaluations of tumor acidosis within *in vivo* tumor models using parametric maps generated with acido CEST MRI. *Mol Imaging Biol.* (2015) 17:488–96. doi: 10.1007/s11307-014-0816-2
101. Chen LQ, Howison CM, Spier C, Stopeck AT, Malm SW, Pagel MD, et al. Assessment of carbonic anhydrase IX expression and extracellular pH in B-cell lymphoma cell line models. *Leuk Lymphoma.* (2015) 56:1432–9. doi: 10.3109/10428194.2014.933218
102. Moon BF, Jones KM, Chen LQ, Liu P, Randtke EA, Howison CM, et al. A comparison of iopromide and iopamidol, two acidoCEST MRI contrast media that measure tumor extracellular pH. *Contrast Media Mol Imaging.* (2015) 10:446–55. doi: 10.1002/cmmi.1647
103. Muller-Lutz A, Khalil N, Schmitt B, Jellus V, Pentang G, Oeltzschner G, et al. Pilot study of Iopamidol-based quantitative pH imaging on a clinical 3T MR scanner. *MAGMA.* (2014) 27:477–85. doi: 10.1007/s10334-014-0433-8
104. Keupp J, Heijman E, Langereis S, Grull H, Longo DL, Terreno E, et al. Respiratory triggered chemical exchange saturation transfer mri for pH mapping in the kidneys at 3T. In: *Proceedings of the 19th Annual Meeting of ISMRM* (Montreal, QC, Canada) (2011). p. 690.
105. Keupp J, Dimitrov I, Langereis S, Togao O, Takahashi M, Sherry A. Non-invasive cest-mri measurement of pH in the human kidneys using an approved ct contrast agent. In: *Proceedings of the 19th Annual meeting of the ISMRM* (Montreal, QC, Canada) (2011). p. 810.
106. Jones KM, Randtke EA, Yoshimaru ES, Howison CM, Chalasani P, Klein RR, et al. Clinical translation of tumor acidosis measurements with AcidoCEST MRI. *Mol Imaging Biol.* (2017) 19:617–25. doi: 10.1007/s11307-016-1029-7
107. Sun PZ, Longo DL, Hu W, Xiao G, Wu R. Quantification of iopamidol multi-site chemical exchange properties for ratiometric chemical exchange saturation transfer (CEST) imaging of pH. *Phys Med Biol.* (2014) 59:4493–504. doi: 10.1088/0031-9155/59/16/4493
108. Jones KM, Randtke EA, Howison CM, Pagel MD. Respiration gating and Bloch fitting improve pH measurements with acidoCEST MRI in an ovarian orthotopic tumor model. *Proc SPIE Int Soc Opt Eng.* (2016) 9788:978815. doi: 10.1117/12.2216418
109. Randtke EA, Granados JC, Howison CM, Pagel MD, Cardenas-Rodriguez J. Multislice CEST MRI improves the spatial assessment of tumor pH. *Magn Reson Med.* (2017) 78:97–106. doi: 10.1002/mrm.26348

110. Wu R, Longo DL, Aime S, Sun PZ. Quantitative description of radiofrequency (RF) power-based ratiometric chemical exchange saturation transfer (CEST) pH imaging. *NMR Biomed.* (2015) 28:555–65. doi: 10.1002/nbm.3284
111. Arena F, Irrera P, Consolino L, Colombo Serra S, Zaiss M, Longo DL. Flip-angle based ratiometric approach for pulsed CEST-MRI pH imaging. *J Magn Reson.* (2018) 287:1–9. doi: 10.1016/j.jmr.2017.12.007
112. Longo DL, Sun PZ, Consolino L, Michelotti FC, Uggeri F, Aime S. A general MRI-CEST ratiometric approach for pH imaging: demonstration of *in vivo* pH mapping with iobitridol. *J Am Chem Soc.* (2014) 136:14333–6. doi: 10.1021/ja5059313
113. Hancu I, Dixon WT, Woods M, Vinogradov E, Sherry AD, Lenkinski RE. CEST and PARACEST MR contrast agents. *Acta Radiol.* (2010) 51:910–23. doi: 10.3109/02841851.2010.502126
114. Delli Castelli D, Ferrauto G, Cutrin JC, Terreno E, Aime S. *In vivo* maps of extracellular pH in murine melanoma by CEST-MRI. *Magn Reson Med.* (2014) 71:326–32. doi: 10.1002/mrm.24664
115. Ferrauto G, Di Gregorio E, Auboiroux V, Petit M, Berger F, Aime S, et al. CEST-MRI for glioma pH quantification in mouse model: Validation by immunohistochemistry. *NMR Biomed.* (2018) 31:e4005. doi: 10.1002/nbm.4005
116. Sheth VR, Li Y, Chen LQ, Howison CM, Flask CA, Pagel MD. Measuring *in vivo* tumor pHe with CEST-FISP MRI. *Magn Reson Med.* (2012) 67:760–8. doi: 10.1002/mrm.23038
117. Liu G, Li Y, Sheth VR, Pagel MD. Imaging *in vivo* extracellular pH with a single paramagnetic chemical exchange saturation transfer magnetic resonance imaging contrast agent. *Mol Imaging.* (2012) 11:47–57. doi: 10.2310/7290.2011.00026
118. Coman D, Huang Y, Rao JU, De Feyter HM, Rothman DL, Juchem C, et al. Imaging the intratumoral-peritumoral extracellular pH gradient of gliomas. *NMR Biomed.* (2016) 29:309–19. doi: 10.1002/nbm.3466
119. Fernando WS, Martins AF, Zhao P, Wu Y, Kiefer GE, Platas-Iglesias C, et al. Breaking the barrier to slow water exchange rates for optimal magnetic resonance detection of paraCEST agents. *Inorg Chem.* (2016) 55:3007–14. doi: 10.1021/acs.inorgchem.5b02850
120. Sonveaux P, Vegran F, Schroeder T, Wergin MC, Verrax J, Rabbani ZN, et al. Targeting lactate-fueled respiration selectively kills hypoxic tumor cells in mice. *J Clin Invest.* (2008) 118:3930–42. doi: 10.1172/JCI36843
121. Semenza GL. Tumor metabolism: cancer cells give and take lactate. *J Clin Invest.* (2008) 118:3835–7. doi: 10.1172/JCI37373
122. Rattigan YL, Patel BB, Ackerstaff E, Sukenick G, Koutcher JA, Glod JW, et al. Lactate is a mediator of metabolic cooperation between stromal carcinoma associated fibroblasts and glycolytic tumor cells in the tumor microenvironment. *Exp Cell Res.* (2012) 318:326–35. doi: 10.1016/j.yexcr.2011.11.014
123. Glunde K, Bhujwalla ZM. Metabolic tumor imaging using magnetic resonance spectroscopy. *Semin Oncol.* (2011) 38:26–41. doi: 10.1053/j.seminoncol.2010.11.001
124. Serrao EM, Brindle KM. Potential clinical roles for metabolic imaging with hyperpolarized [1-^{13}C]pyruvate. *Front Oncol.* (2016) 6:59. doi: 10.3389/fonc.2016.00059
125. Brindle KM. Imaging metabolism with hyperpolarized (13)C-labeled cell substrates. *J Am Chem Soc.* (2015) 137:6418–27. doi: 10.1021/jacs.5b03300
126. Viale A, Reineri F, Dastru W, Aime S. Hyperpolarized (13)C-pyruvate magnetic resonance imaging in cancer diagnostics. *Expert Opin Med Diagn.* (2012) 6:335–45. doi: 10.1517/17530059.2012.687372
127. Reineri F, Daniele V, Cavallari E, Aime S. Assessing the transport rate of hyperpolarized pyruvate and lactate from the intra- to the extracellular space. *NMR Biomed.* (2016) 29:1022–7. doi: 10.1002/nbm.3562
128. Hovener JB, Pravdivtsev AN, Kidd B, Bowers CR, Gloggler S, Kovtunov KV, et al. Parahydrogen-Based Hyperpolarization for Biomedicine. *Angew Chem Int Ed Engl.* (2018) 57:11140–62. doi: 10.1002/anie.201711842
129. Durst M, Koellisch U, Daniele V, Steiger K, Schwaiger M, Haase A, et al. Probing lactate secretion in tumours with hyperpolarised NMR. *NMR Biomed.* (2016) 29:1079–87. doi: 10.1002/nbm.3574
130. DeBrosse C, Nanga RP, Bagga P, Nath K, Haris M, Marincola F, et al. Lactate chemical exchange saturation transfer (LATEST) imaging *in vivo* A biomarker for LDH activity. *Sci Rep.* (2016) 6:19517. doi: 10.1038/srep19517
131. Saito S, Takahashi Y, Ohki A, Shintani Y, Higuchi T. Early detection of elevated lactate levels in a mitochondrial disease model using chemical exchange saturation transfer (CEST) and magnetic resonance spectroscopy (MRS) at 7T-MRI. *Radiol Phys Technol.* (2019) 12:46–54. doi: 10.1007/s12194-018-0490-1
132. Aime S, Delli Castelli D, Fedeli F, Terreno E. A paramagnetic MRI-CEST agent responsive to lactate concentration. *J Am Chem Soc.* (2002) 124:9364–5. doi: 10.1021/ja0264044
133. Zhang L, Martins AF, Zhao P, Tieu M, Esteban-Gomez D, McCandless GT, et al. Enantiomeric recognition of d- and l-lactate by CEST with the aid of a paramagnetic shift reagent. *J Am Chem Soc.* (2017) 139:17431–7. doi: 10.1021/jacs.7b08292
134. Zhang L, Martins AF, Mai Y, Zhao P, Funk AM, Clavijo Jordan MV, et al. Imaging extracellular lactate *in vitro* and *in vivo* using CEST MRI and a paramagnetic shift reagent. *Chemistry.* (2017) 23:1752–6. doi: 10.1002/chem.201604558

Conflict of Interest: The authors declare that the research was conducted in the absence of any commercial or financial relationships that could be construed as a potential conflict of interest.